Experimental evidence for long-distance electrodynamic intermolecular forces

Mathias Lechelon, Yoann Meriguet, Matteo Gori, Sandra Ruffenach, Ilaria Nardecchia, Elena Floriani, Dominique Coquillat, Frederic Teppe, Sébastien Mailfert, Didier Marguet, et al.

PHYSICAL SCIENCES

Experimental evidence for long-distance electrodynamic intermolecular forces

Mathias Lechelon[1,2,3], Yoann Meriguet[4,5], Matteo Gori[1,2,6], Sandra Ruffenach[5], Ilaria Nardecchia[1,2,3], Elena Floriani[1,2], Dominique Coquillat[5], Frédéric Teppe[5], Sébastien Mailfert[3], Didier Marguet[3], Pierre Ferrier[3], Luca Varani[4], James Sturgis[7], Jeremie Torres[4]*, Marco Pettini[1,2]*

Both classical and quantum electrodynamics predict the existence of dipole-dipole long-range electrodynamic intermolecular forces; however, these have never been hitherto experimentally observed. The discovery of completely new and unanticipated forces acting between biomolecules could have considerable impact on our understanding of the dynamics and functioning of the molecular machines at work in living organisms. Here, using two independent experiments, on the basis of different physical effects detected by fluorescence correlation spectroscopy and terahertz spectroscopy, respectively, we demonstrate experimentally the activation of resonant electrodynamic intermolecular forces. This is an unprecedented experimental proof of principle of a physical phenomenon that, having been observed for biomacromolecules and with long-range action (up to 1000 Å), could be of importance for biology. In addition to thermal fluctuations that drive molecular motion randomly, these resonant (and thus selective) electrodynamic forces may contribute to molecular encounters in the crowded cellular space.

INTRODUCTION

Beyond the strong interest for fundamental physics in observing intermolecular dipole-dipole electrodynamic (ED) forces, this experimental study to detect these forces was highly motivated by their possible role at the molecular level in biology. From a physicist's point of view, living matter offers a wealth of fascinating dynamic phenomena involving biomolecules (proteins and nucleic acids) organized in an intricate and complex network of biochemical interactions providing astonishing efficiency. In numbers, a human cell at any given time may contain about 130,000 binary interactions between proteins (*1*), of which about 34,000 unique human protein-protein interactions are already listed on databases (*2*). The forces hitherto considered in biological contexts are of (quasi-) electrostatic nature (chemical and hydrogen bonds, bare Coulomb, van der Waals London, and Hamaker forces) and are limited to a range of actions shorter than 10 Å due to Debye screening by small freely moving ions in the intracellular water. Such interactions are relevant for stereospecific, "lock-and-key," and "induced-fit" interactions at short distances but hardly effective to recruit distant molecules. Thus, understanding how the right molecule gets to the right place, at the right moment, in the right cascade of events of any biological action is one of the most notable challenges. Fundamentally, it is assumed that this network of interactions is dominated by random molecular diffusion throughout the cellular spaces in which, sooner or later, a molecule will encounter its cognate partners. However, free diffusion is considerably slowed down in a highly crowded environment (*3*) as in the case of the cell interior. Moreover, when diffusion measurements are performed in complex molecular organizations such as those of living cells, most of the biomolecules show anomalous rather than Brownian diffusion (*4*, *5*). Furthermore, structuring of the cytosol into phase-separated domains (*6*, *7*), substrate channeling of the metabolons (*8*), or long-distance interactions in DNA searching (*9*) and organization (*10*) has recently come to the forefront to question the discrepancy between the observed reaction rates in cells and the predictions of a strict random diffusion model (*6*, *11*). Within this framework, dipole-dipole ED interactions are predicted to promote molecular attraction by being selective through resonance and to act over long distances (*12*). These forces can propagate without attenuation in electrolytes of ionic strength comparable to that in the cytoplasm, provided that their oscillation frequency exceeds the Maxwell frequency at few hundreds of megahertz (*13*), since at such frequencies, the Debye screening is ineffective (*14*). Therefore, we hypothesize that, in addition to random diffusion, selective long-range attractive ED interactions increase the encounter rates between *A* and *B* cognate partners through a mutual force field described by a potential $U(r)$, where r is the intermolecular distance. Then, after the Smoluchowski-Debye formula (*15*, *16*), the association rate is given by $k_a^* = 4\pi R^*(D_A + D_B)$, where $D_{A,B}$ are their diffusion coefficients and R^* is given by

$$R^* = \left[\int_{R_A+R_B}^{\infty} \frac{e^{U(r)/kT}}{r^2} dr \right]^{-1} \tag{1}$$

where R_A and R_B are the hydrodynamic radii of *A* and *B*, respectively, k is the Boltzmann constant, and T the temperature. For an attractive interaction, $U(r) < 0$, Eq. 1 implies that $k_a^* > k_a = 4\pi(R_A + R_B)(D_A + D_B)$, that is, an increase of the association rate with respect to the purely diffusive k_a. However, ED macromolecular interactions have not previously been considered for several reasons, including the following: (i) They have never been observed in any experimental

[1]Aix-Marseille Univ., Université de Toulon, CNRS, Marseille, France. [2]Centre de Physique Théorique, CNRS, Marseille, France. [3]Centre d'Immunologie de Marseille-Luminy, Aix-Marseille Univ., CNRS, Inserm, Marseille, France. [4]Institut d'Electronique et des Systèmes, University of Montpellier, CNRS, Montpellier, France. [5]Laboratoire Charles Coulomb, University of Montpellier, CNRS, Montpellier, France. [6]Quantum Biology Lab, Howard University, 2400 6th St NW, Washington, DC 20059, USA. [7]Laboratoire d'Ingenierie des Systèmes Macromoléculaires, Aix-Marseille Univ., CNRS, Marseille, France.
*Corresponding author. Email: jeremie.torres@umontpellier.fr (J.T.); marco.pettini@cpt.univ-mrs.fr (M.P.)

context, although theoretically predicted by both classical (*12, 17*) and quantum electrodynamics (*18*); (ii) they require an out-of-equilibrium system (*12*), which, although, of course, found in all living systems, is hard to organize in the laboratory in vitro, especially with molecules in metastable states with strongly excited giant dipole vibrations, as required for such interactions; (iii) out-of-equilibrium collective vibrations of macromolecules are expected in the 0.1 to 1.0 THz domain, and this is experimentally challenging to observe because of the strong absorption of water, and such vibrations have only recently been detected (*19*) and corroborated by theoretical studies (*20, 21*). The coherence of these collective molecular vibrations is theoretically expected to be long lived (*22*).

Here, we demonstrate experimentally the activation of long-range attractive ED forces between proteins. This was made possible through the study of R-phycoerythrin (R-PE), a protein that can be excited naturally by an external energy supply, a light source. Then, by working at different concentrations (i.e., intermolecular distances) and excitation power of a laser as the light source, we have achieved the following: (i) observation of the activation of collective intra-molecular oscillation of the proteins, a necessary prerequisite to activating the physical mechanism pictorially outlined in Fig. 1A; (ii) observation of a distributed-clustering transition dependent on activation of these collective molecular oscillations, as expected after a thorough preparatory work (*3, 23, 24, 25*); and (iii) the consequent expected change of the frequency of the collective oscillation (*26*). For this, two experimental techniques were used: terahertz (THz) spectroscopy, mainly composed of two setups using either a THz rectenna or a microwire probe as sensors, respectively (see Materials and Methods for details), and fluorescence correlation spectroscopy (FCS) (Fig. 1, B and C). Overall, our experimental work supports a proof of principle that out-of-equilibrium collective oscillations are capable of activating dipole-dipole ED intermolecular forces, thus paving the way for exploring the potential role of ED intermolecular forces in living matter.

RESULTS

This first experimental study has been performed with a natural light-harvesting protein derived from red algae, the R-PE (see fig. S1). This protein is a hexamer $(\alpha\beta)_6\gamma$, where the subunit α contains two phycoerythrobilins, the subunit β contains three phycoerythrobilins and one phycourobilin, and the γ subunit contains two or three phycoerythrobilins and one or two phycourobilins. That is, some limited variability in the number of fluorochromes is possible and 38 fluorochromes are considered a typical number. All these subunits form one of the brightest fluorescent dyes (the entire protein) hitherto found. These pigments are highly sensitive to the $\lambda = 488$-nm light used in these experiments.

Thus, under suitable illumination conditions (details in Materials and Methods) of the R-PE molecules in saline solution, each molecule can enter a coherent vibrational state (Fig. 2), displaying similar phenomena to those reported for bovine serum albumin (BSA) protein in (*19*): the existence of a threshold for the energy input rate to activate the collective mode and a saturation of the oscillation amplitude at high values of the energy input rate. In this saturation regime, two collective oscillation frequencies for R-PE are found (details in Materials and Methods and the Supplementary Materials). One at 0.071 THz (=2.4 cm^{-1}) and another at 0.096 THz (=3.2 cm^{-1}), the latter is only observable under specific saturation conditions of

the lower frequency peak (see Fig. 3). Even if a protein is not an idealized solid, or of strictly well-defined shape, considering the best fitting simple geometric shape provided a successful precedent with the BSA. The BSA is referred to as a globular protein, and it is certainly not a rigid, elastic, solid sphere, but by applying a formula for the spheroidal modes of an elastic sphere, an excellent agreement with the experimental finding was obtained (*19*). Similarly, the geometric shape that best fits the hexamer form of the R-PE is a torus. Even if such a treatment of R-PE and BSA collective vibration modes is somewhat rudimentary, it provides information adequate to what is needed in the present context. Schematizing the R-PE protein as a torus-shaped object of $M = 240$ kDa, with a larger midline radius $R = 37.5$ Å, a minor radius $r = 30$ Å (*27*), density ρ (the ratio between M and the volume of the torus), and Young elastic modulus E, the frequencies of the collective extension modes (those corresponding to oscillating larger radius R) are given in (*28*)

$$\nu_n = \frac{(1 + n^2)^{1/2}}{2\pi R} \left(\frac{E}{\rho}\right)^{1/2} \tag{2}$$

Hence, the ratio $\nu_1/\nu_0 = \sqrt{2} \simeq 1.41$, which approximates within a 4% the ratio between the observed frequencies, that is, $0.096/0.071 = 1.35$. The Young modulus of R-PE is not known in the literature, but by inverting the above formula, we obtain $E \simeq 5.3$ GPa, which seems reasonable knowing that at 300 K for myoglobin $E \simeq 3.5$ GPa and for BSA $E \simeq 6.75$ GPa (*29*) (both proteins being mostly made of α-helices like R-PE). Such an empirical approach gives a useful insight on the observed phenomenology as it was successfully done for the BSA (*19*).

A theoretically expected signature of attractive ED forces among macromolecules vibrating at the same frequency is a phase transition between a dispersed phase of rapidly diffusing molecules and a clustered phase of very slowly moving aggregates of molecules (see the Supplementary Materials) (*24*). The control parameter of this transition is the average intermolecular distance, which is set by adjusting the molecular concentration.

In the FCS experiments, the protein concentrations $\mathcal{C}$ have been varied in the interval between 0.1 and 10 µM to make the average intermolecular distance $\langle r \rangle = \mathcal{C}^{-1/3}$ vary in the interval of 550 to 1950 Å.

The ionic strength of the protein solution is kept at 200 mM by means of suitable concentrations of NaCl in water. This ensures a good shielding of electrostatic interactions. Moreover, the laser power ($\lambda = 488$ nm) has been varied between 50 and 150 µW. Typical fluorescence traces are reported for different laser powers and protein concentrations (figs. S4 and S5).

The diffusion times τ_D determined from the cross-correlation functions (CCFs) of fluorescence traces, and the measured waist of the confocal volume where the molecules are both excited and observed, allow estimation of the diffusion coefficients D. The use of CCFs is motivated in Materials and Methods and figs. S2 and S3. The values of the diffusion coefficient D are normalized with respect to the Brownian values D_0 of each data series recorded at a given laser power (Fig. 4). At low laser power, the measured value of D_0 matches the expected theoretical one $D_0 = k_B T/(6\pi\eta R_H)$, where η is the viscosity of the solution, and R_H is the hydrodynamic radius of the protein. At a laser power of 50 µW, the observed values of D (blue circles) do not change with the intermolecular distance. The diffusion of the R-PE molecules is Brownian for all the concentrations
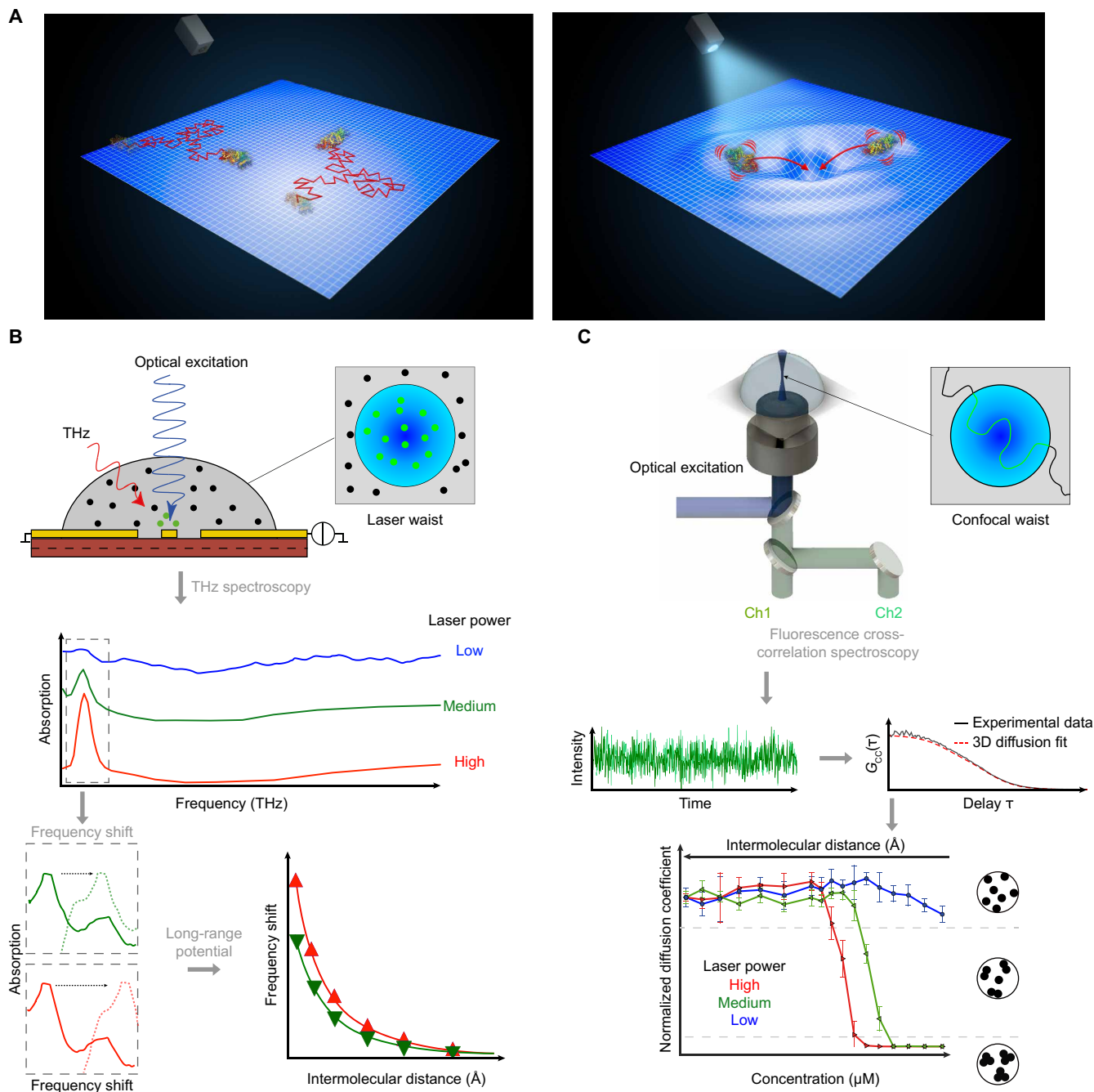
Fig. 1. Long-range ED interactions: Principle and experimental approaches. (**A**) At thermal equilibrium, macromolecules show a Brownian diffusive motion in solution (left). By switching-on an external energy source, molecules are in an out-of-thermal equilibrium collective vibrational state that can generate ED forces through associated large dipolar resonant oscillations (right). (**B**) In THz spectroscopy, the frequency of the collective vibration varies as a function of the average intermolecular distance (determined by the protein concentration). With respect to the reference frequency at "infinite" dilution, a frequency shift inversely proportional to the cubic power of the average intermolecular distance is theoretically expected if the proteins interact through ED forces. (**C**) In FCS, the transit times of the proteins across the volume of observation are measured and, hence, the protein diffusion coefficients. Under out-of-thermal equilibrium conditions, the theory predicts a phase transition due to ED forces clustering proteins. This should be observed at a given protein concentration by a sudden drop in the diffusion coefficient from its Brownian value. In both (B) and (C), out-of-thermal equilibrium is activated by optical excitation.
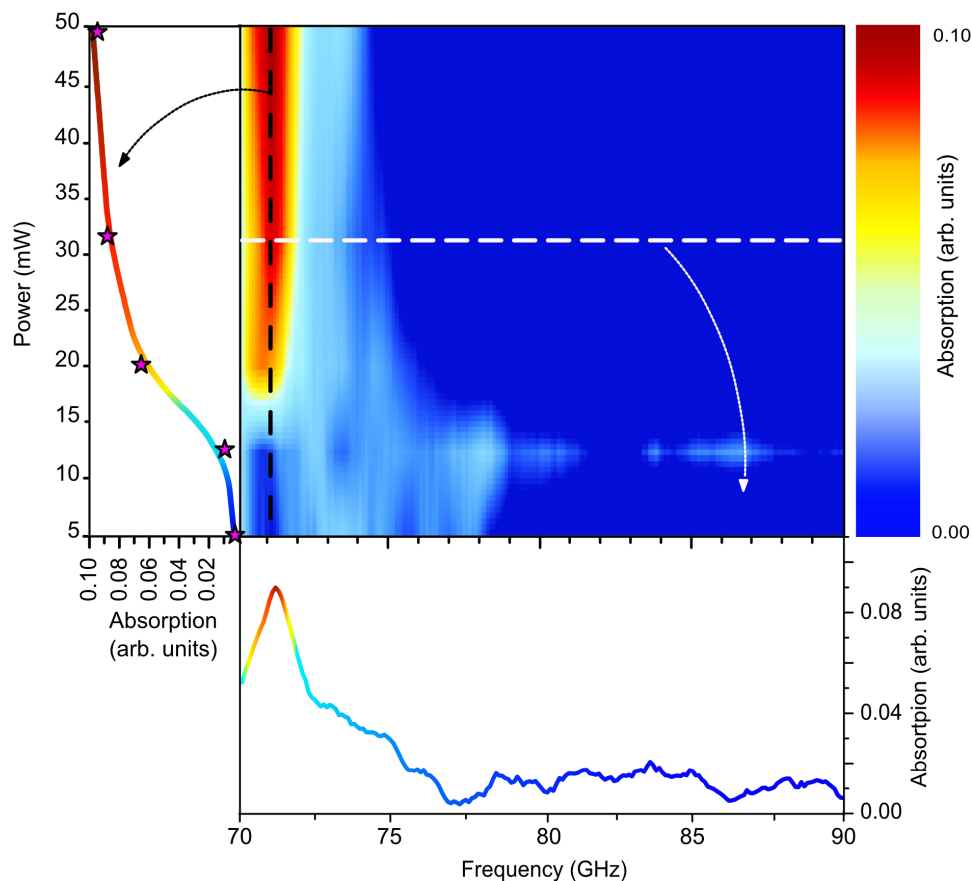
Fig. 2. Collective oscillation of the R-PE measured by THz spectroscopy. Absorption strength of the R-PE (1 mg/ml in 200 mM NaCl) as a function of detection frequency and the laser power activating the molecular collective oscillation at a frequency of 71 GHz (2.4 cm^{-1}). The absorption line profile (bottom) indicated by the horizontal white dashed line was measured at an optical power of 31.5 mW, while the laser power threshold (left) behavior is indicated by the black dashed line. Stars stand for experimental data, and the interpolating line is just a guide to the eye.
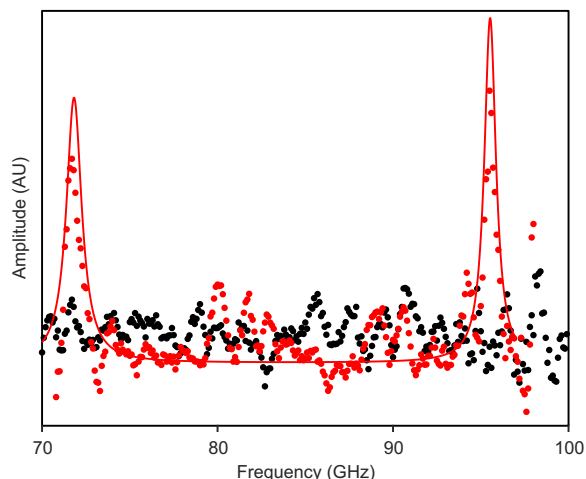

Fig. 3. R-PE coherent vibrational states. Comparison of the R-PE in saline solution (red) and saline solution without R-PE (black). Two collective extension modes of R-PE appear at 71 and 96 GHz. Experimental data are indicated by full circles, and Lorentz fit is indicated by a solid line. AU, arbitrary units.

considered. This means that either the energy input rate is below the threshold value required to excite molecular collective vibrations or the intermolecular ED forces are very weak because of the small amplitude of the collective vibrations of the R-PE proteins. The mismatch between the laser power values mentioned in Fig. 2 for THz experiments and those reported above for diffusion experiments is due to the different volumes illuminated (see Materials and Methods).

At higher laser power, 100 μW, obviously and consistently with a thermal effect, the measured value of D_0 at low concentration is larger than in the preceding case. However, it cannot explain, in the interval of intermolecular distances 700 to 750 Å (green triangles), the steep drop of D/D_0 that correlates with the increase of the fluorescence fluctuations and a sudden increase of the diffusion time τ_D.

At the highest laser power considered, 150 μW, again, the steep drop of D/D_0 is observed but now in the interval of intermolecular distances of 900 to 950 Å (red triangles). In both cases, the steep drop of D/D_0 correlates with a strong increase of the fluorescence fluctuations and a sudden and huge increase by several orders of magnitude of the diffusion time τ_D. The strong increase of the fluorescence fluctuations is shown in fig. S6, where, for instance, at an average intermolecular distance of 600 Å, the variance of the
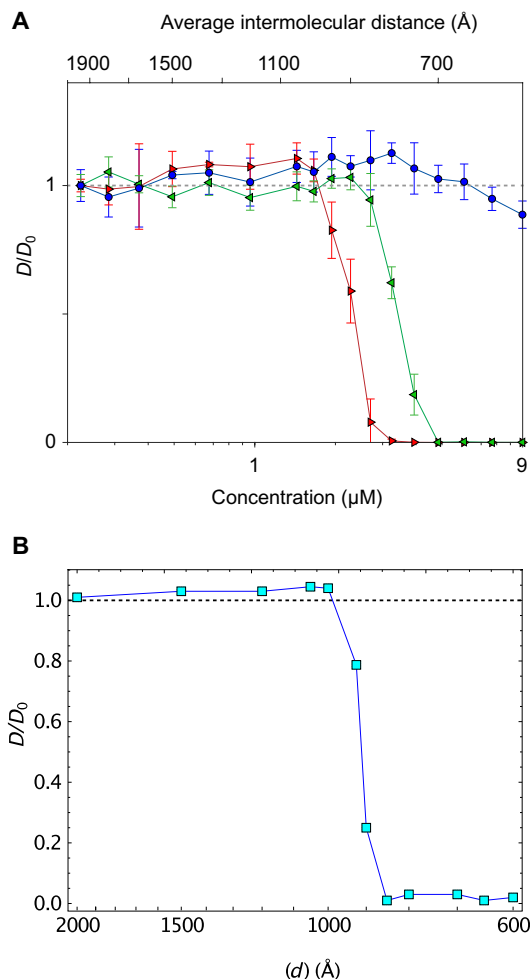
A

B

Fig. 4. Effect of protein concentration and laser power illumination on R-PE diffusion: Clustering phase transition. (**A**) Diffusion coefficients normalized to the Brownian D_0 values measured for each data series at 0.223 μM ($\langle r \rangle \simeq 1950$ Å) and recorded at 50 (blue circles), 100 (green triangles), and 150 μW (red triangles). Each point corresponds to the average of five independent experiments. (**B**) Molecular dynamics computation of self-diffusion coefficient D/D_0 (normalized to the Brownian value D_0) versus intermolecular average distance $\langle d \rangle$ for a system of particles in a cubic box interacting through long-range ED forces.

fluorescence fluctuations is more than five orders of magnitude larger than the same quantity measured at an average intermolecular distance of 1950 Å. Correspondingly, the diffusion times measured through the correlation functions that are reported in the right lower panel of fig. S7 are 4.9 s and 4.8×10^{-5} s at an average intermolecular distance of 600 and 1950 Å, respectively.

The steep drop of D/D_0 and the increased amplitude of fluorescence fluctuations are the observable effects of a clustering phase transition stemming from the competition between the ED intermolecular attractive forces and thermal fluctuations. This is confirmed theoretically by a semi-analytical model (Fig. 4B), by molecular dynamics simulations, and by Monte Carlo computations (see the Supplementary Materials).

Molecular dynamics simulations have been done to estimate the effect of long-range ED interactions on the self-diffusion coefficient D of a system of interacting molecules defined by

$$D = \lim_{t \to +\infty} \frac{\langle \|\Delta \boldsymbol{r}_i(t)\|^2 \rangle_i}{6t} \quad (3)$$

where $\Delta \boldsymbol{r}_i(t)$ is the displacement at time t of the i-th molecule with respect to its initial position and $\langle \cdot \rangle_i$ is the average over all the particles in the system. This is the physical quantity measured by means of FCS experiments, thus allowing a direct comparison between the outcomes of numerical simulations and the outcomes of laboratory experiments.

The dynamics is described by the Langevin equations in the overdamped limit (without inertial terms)

$$\frac{\mathrm{d}\boldsymbol{r}_i}{\mathrm{d}t} = -\frac{1}{\gamma} \nabla_{\boldsymbol{r}_i} \sum_{j \neq i} U(\|\boldsymbol{r}_i - \boldsymbol{r}_j\|) + \sqrt{\frac{2 k_B T}{\gamma}} \xi_i(t) \ \forall i = 1,..,N \quad (4)$$

where γ is the viscous friction constant, U is the ED interaction potential, T is the temperature of the solution, and $\xi_i(s)$ is a noise term accounting for the random collisions of water molecules, s.t.

$$\langle \xi_{A,i}(t) \rangle_t = 0 \ \langle \xi_{A,i}(t) \xi_{B,j}(t') \rangle_t = \delta(t - t') \, \delta_{AB} \delta_{i,j} \, \forall i, j = 1,\dots,N$$
$$\forall A, B = 1,\dots,3.$$

The parameters entering the model are chosen to reproduce the experimental conditions (details are in the Supplementary Materials), and the sudden drop of the diffusion coefficient is found in correspondence with the formation of clusters at an average intermolecular distance in agreement with the experimental finding at 150 μW in Fig. 4A. In Fig. 5, two snapshots are shown of numerical Monte Carlo computations performed by considering long-range ED interparticle forces. Thus, the appearance of clusters predicted theoretically has been experimentally observed through the sudden enhancement of fluorescence fluctuation amplitudes and long transit times across the confocal volume of the FCS setup. Clusters of R-PE were visually evidenced by fluorescence microscopy in Fig. 6 and movies in the Supplementary Materials.

In increasing the laser power, the higher the power, the stronger the collective oscillation of R-PE molecules and the larger the associated oscillating dipole moment, hence the displacement of the clustering transition to a greater average intermolecular distance for stronger molecular oscillations. Consistently, by suddenly lowering the power of the laser light supply in the clustered phase, a rapid disaggregation of the clusters is observed, as shown by the sequences of frames reported in Fig. 6. Note that the frame on the top left of this figure shows that under the same conditions of temperature and particle concentration, when the energy input rate is below the threshold value to activate intramolecular collective vibrations, the clustering transition disappears.

All these results are a clear-cut proof of the activation of ED intermolecular attractive forces due to the collective vibrations of the R-PE molecules.

An independent confirmation of the activation of ED intermolecular attractive forces is obtained by measuring the shift of the collective vibrational frequency as a function of the concentration of molecules. Once again, the proteins were observed in aqueous solution with the addition of 200 mM NaCl to screen electrostatic interactions. Theory predicts that ED dipole-dipole interaction between two molecules results in a shift $\Delta \nu$ of their vibration frequency from the unperturbed frequency ν_0, a shift proportional to $1/r^3$ with r being the intermolecular distance (*12*). This law is preserved
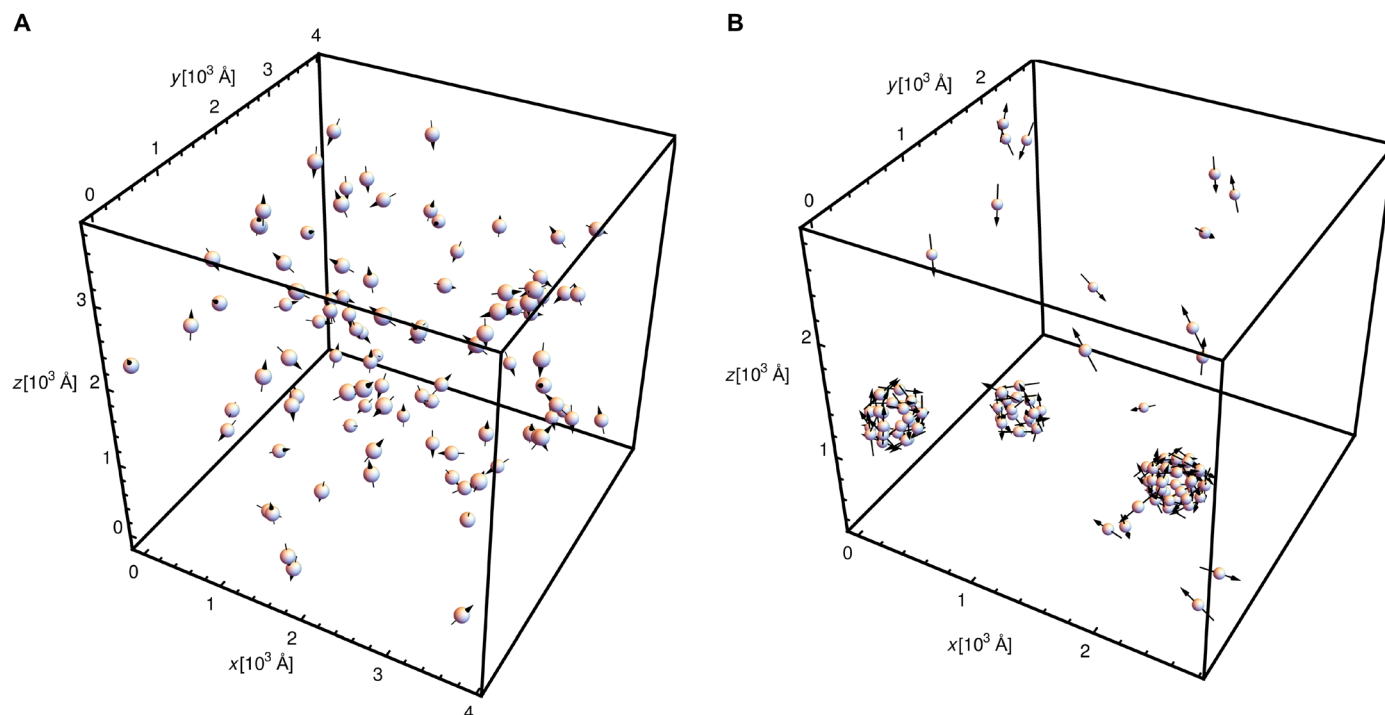
Fig. 5. Snapshots of numerical Monte Carlo computations. Clustering transition induced by long-range ED interparticle forces observed by changing the initial value of $\langle r \rangle$. (**A**) With $\langle r \rangle_{initial} \simeq 1000$ Å, the system remains in the dispersed phase where $D/D_0 = 1$ (Brownian diffusion). (**B**) With $\langle r \rangle_{initial} \simeq 950$ Å, the system switches to the clustered phase, where D/D_0 is very small.

also for a large number of interacting molecules, that is, the frequency shift is proportional to $1/\langle r \rangle^3$, where $\langle r \rangle$ is the average intermolecular distance given by $\langle r \rangle = C^{-1/3}$ (see the Supplementary Materials for the theoretical explanation). The unperturbed vibration frequency ν_0 is operationally measured at very low molecular concentrations. The shifts $\Delta \nu$ are then measured with respect to this value of ν_0.

The collective oscillation frequency of the R-PE at 0.071 THz (i.e., 2.4 cm^{-1}) allowed to use as THz detector an electronic nanodevice, namely, a bow-tie antenna on the two-dimensional (2D) electron gas layer of a field-effect transistor (FET) called a rectenna (see Materials and Methods) (30). The measured frequency shift is found to follow a linear dependence on the protein concentration, that is, the experimental outcomes are in excellent agreement with the theoretical predictions (Fig. 7A). The steepening of the fitted lines in Fig. 7A as laser power is increased is also in agreement with expectations. This is because the increasing oscillation amplitude (entailing a larger oscillating dipole moment) results in stronger intermolecular ED interaction and hence a larger frequency shift (for theoretical details, see the Supplementary Materials). The case of R-PE is especially important because two independent experimental approaches lead to the same physical conclusion: the activation of intermolecular ED forces acting at a long distance. Thus, the possibility of artefacts or misinterpretations is ruled out. These forces are not peculiar to the R-PE because they are also observed by making measurements with another protein, BSA. BSA molecules were labeled with an average number of five fluorochromes AF488 5-tetrafluorophenyl ester, covalently bonded to the lysine residues, excitable by the light emitted by a diode laser at 488 nm. The reason for considering the BSA is twofold: First, the labeled BSA molecules,

when continuously supplied by laser light at λ = 488 nm, are driven in a collective vibration mode at 0.314 THz (i.e., 10 cm^{-1}) (19); second, R-PE and BSA both have a structure composed largely of α-helices (fig. S1), a property that we can suppose to be facilitating the activation of collective vibrational modes. α-Helices behave as springs undergoing the so-called accordion modes; therefore, a protein mainly composed of α-helices is reasonably supposed to be highly flexible and its components can undergo synchronization phenomena, possibly giving rise to a collective oscillation.

The collective oscillation frequency of the BSA at 0.314 THz required the use of a near-field microwire-based probe coupled with a waveguide (see Fig. 8B). Again, the measured frequency shift is found to follow a linear dependence on the protein concentration as expected (Fig. 7B). This provides a remarkable confirmation of the activation of long-distance ED interactions also for BSA.

It is worth pointing out that the two THz experimental setups have been operated at a different spatial density of the laser light, with respect to diffusion experiments, to prevent a clustering transition during the frequency shift measurements. By using a set of optical density (OD) filters to lower the spatial density of the laser power, the ED forces can be weakened to the point of being unable to entail the clustering transition by overcoming thermal noise and the protein molecules that keep diffusing with a Brownian motion (see Materials and Methods).

DISCUSSION

In the work presented here, we have experimentally shown that the excitation of out-of-equilibrium collective oscillations is capable of driving molecular association through the activation of ED
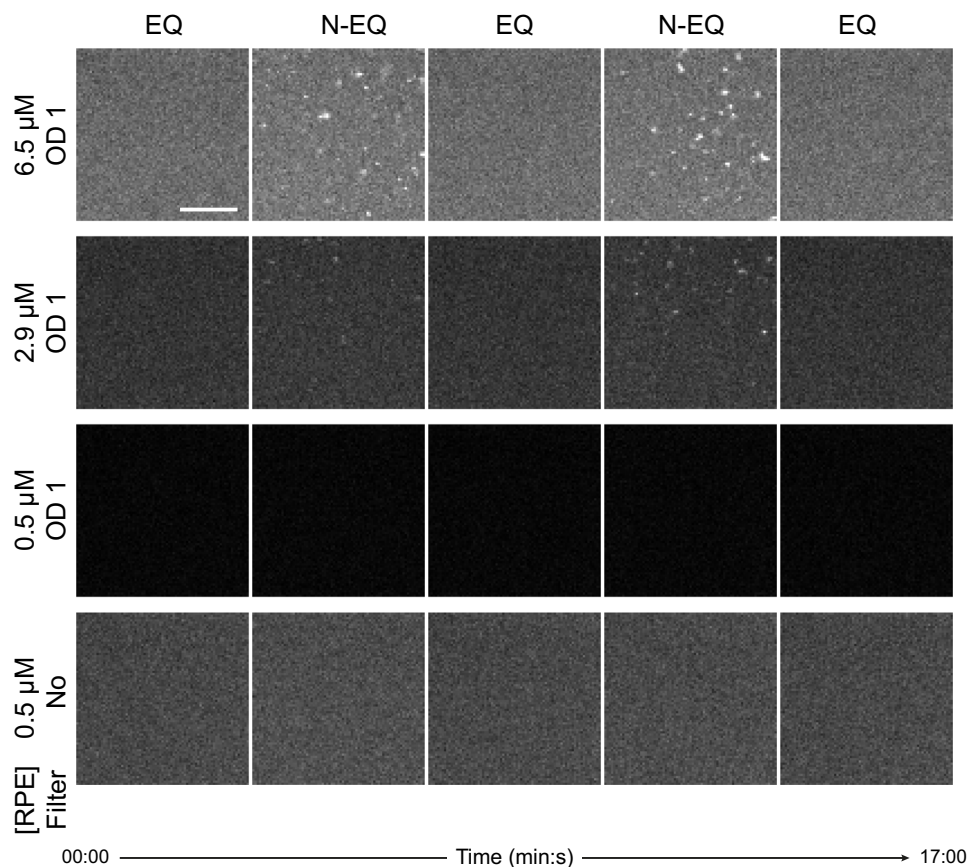
Fig. 6. Screenshots from supplementary videos of a solution of R-PE under laser light illumination. Optical power alternatively varying in time at 50 and 150 μW. EQ stands for proteins at equilibrium (switch-off of collective oscillations) and N-EQ for out of equilibrium (switch-on of collective oscillations). Snapshots have been taken for a concentration of 0.5 μM (average molecular distance of $\langle d \rangle = 1500$ Å) with and without OD filter showing the absence of cluster formation at low concentration. At concentrations of 2.9 μM ($\langle d \rangle = 800$ Å) and 6.5 μM ($\langle d \rangle = 630$ Å), the formation of protein clusters and their reversibility are well evident. The increase of the background brightness in the upper sequence of frames is due to the combined effects of the increase of protein concentration and of the laser power. Scale bar, 10 μm. The units of the time scale are expressed in minute:seconds.

intermolecular forces. R-PE provides convincing evidence for these forces using a pair of complementary experimental approaches. Thus, R-PE represents the "Rosetta stone," allowing us to identify attractive intermolecular forces through two completely different physical effects.

Long-range ED interactions have also been activated using a second protein, fluorescent dye–labeled BSA. These results confirm the generality of this phenomenon, thus paving the way for the experimental searching of ED forces in the more complex environment encountered in cell biology.

A central feature of the ED forces activated by collective molecular vibrations is their long-range property, that is, they stem from an interaction potential decreasing as the third inverse power of the intermolecular distance. This generates first-order phase transitions with the formation of molecular condensates. A thorough theoretical analysis of this transitional behavior, and of the frequency shift of the collective vibrations of the proteins, caused by their interaction through ED forces, can be found in the Supplementary Materials.

By being dynamic and reversible, ED forces can be instrumental in structuring the mesoscale molecular organization through the formation of biomolecular condensates and thus provide a rationale to explain the speed of many cellular processes. While we have

evidence of the association of biological macromolecules driven by ED forces in vitro, the conditions are far from the ones found in cellulo. Here, the energy sources necessary to maintain the molecules out of equilibrium need to be characterized. Among the potential candidates, there are adenosine triphosphate (ATP) as a universal biological fuel, ionic currents such as those used to drive ATP synthesis, ionic collisions, photons produced by mitochondria, or external light (*31*, *32*). The notion of selectivity of ED forces will also need to be explored in a crowded environment composed of a vast diversity of molecular components. More specifically, it will be important to consider the possible role of ED forces between different molecular species (ligand receptor and DNA protein) coresonating at one or more collective oscillation frequencies. Recent numerical studies have shown that correlations of electronic density fluctuations can extend up to 30 in protein-solvent systems (*33*). These correlations, responsible for long-range many-body van der Waals interactions, by structuring hydration layers, could support and give a contribution also to ED intermolecular interactions and communications among biomolecules.

Moreover, our findings could be of general interest for methodological applications requiring tight control in the space and time of molecular interactions in living cells to decipher cellular functions
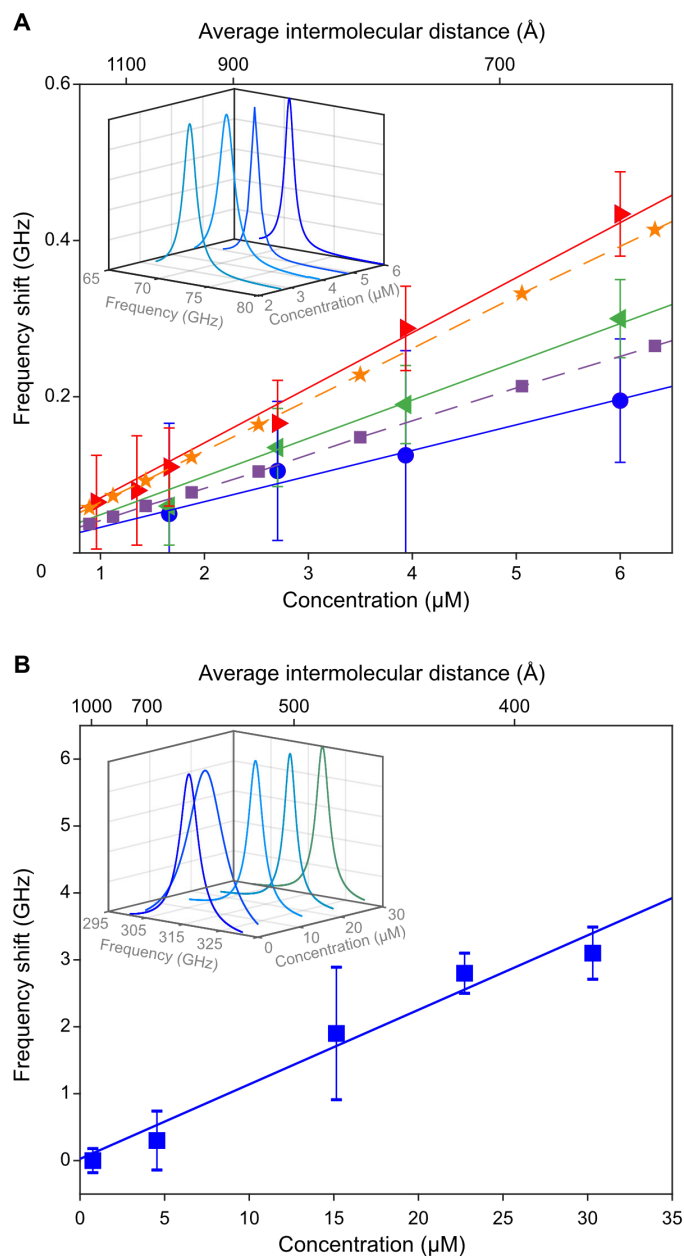
A

B

Fig. 7. Frequency shifts of the intramolecular collective vibrations of R-PE and BSA at different concentrations. Measurements were performed at room temperature in aqueous solution with 200 mM of NaCl. (**A**) R-PE. The shift is relative to the reference frequency measured at the lowest protein concentration. Measurements have been performed at different powers of the laser: 31.5 (blue circles), 39.5 (green triangles), and 50 mW (red triangles). Purple squares and orange stars refer to theoretical outcomes worked out with different values of molecular dipole moments (see the Supplementary Materials). (**B**) BSA at a laser power of 40 mW. Insets: The frequency shifts are measured through a Lorentz fitting of the experimental resonances. The different colors in the insets are just a visual help.

(e.g., in the developing field of optogenetics where molecular interactions are switched on/off by engineered proteins controlled by light) (*34*).

Further, ED forces could also be exploited in the domain of drug design. It has been hypothesized that combining steric complementarity with "long-range complementarity" could improve therapeutic
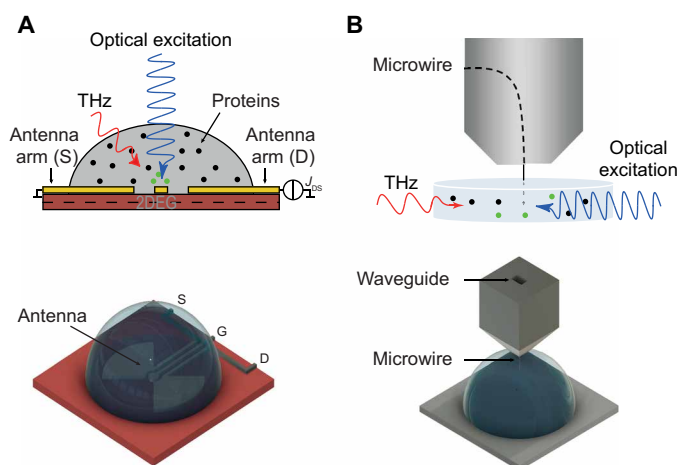
A

B

Fig. 8. THz spectroscopy experimental setups. (**A**) Rectenna for the 0.07 to 0.11 THz band. (**B**) Microwire-based probe for the 0.25- to 0.37-THz band.

efficiency. Thus, ED forces could allow recognition at a distance and drive an efficient mutual approach between a drug and its therapeutic target before their final chemical binding (*35*).

Last, throughout evolution, life has exploited all the available physical laws, processes, and phenomena. It is thus exciting to speculate how the new phenomenon reported here has been used to gain adaptive advantage and possibly overcome some of the adverse effects of molecular crowding in cells.

MATERIALS AND METHODS
Theoretical rationale
A crucial condition to activate long-range ED forces between biomolecules is to put them out of thermal equilibrium, in a coherent vibrational state of all, or a large fraction, of their atoms. At thermal equilibrium a macromolecule "flickers," that is, it undergoes incoherent and random deformations of all its subunits, resulting in small noisy variations of its static dipole moment. At equilibrium, energy equipartition among the normal modes of vibration holds; thus, the amplitude of collective modes is very small. Collective modes have been detected at equilibrium already a long time ago for proteins (*36*) and polynucleotides (*37*) with Raman and far-infrared spectroscopy. However, by keeping a macromolecule out of thermal equilibrium by means of an external energy supply, a phonon condensation phenomenon can be activated (*19*), consisting of the channelling of the supplied energy into a low-frequency coherent mode of vibration of all the atoms (or of a substantial fraction of them) of the same macromolecule. So excited, the macromolecule may have a very large oscillating dipole moment. In turn, in such a collective oscillation state, a biomolecule could activate a long-range attractive ED interaction with other molecules if they have a proper frequency close to that of the coherent mode. This scenario has been proposed a long time ago (*17*, *38*, *39*, *40*) but has been marginalized for several reasons, including its quantum mechanical formulation and because it has never been given experimental evidence. Reformulated in a classical framework (*12*, *19*), the above sketched scenario has been given new credit after the recent experimental proof of the possibility of activating a stationary oscillation of a macromolecule out of thermal equilibrium (*19*). This is a necessary precondition

to activate long-range ED interactions (*12*). It is worth mentioning that in a recent work, it has been convincingly maintained that a full understanding of Fröhlich condensation can come solely from a quantum theory (*22*).

Theoretical design of the experiments

Classical methods for measuring the forces between molecules and characterizing them, such as atomic force microscopy or optical tweezers, even if they give very interesting results on molecular interactions, are not the most obvious and easy to implement in the specific cases of out-of-equilibrium oscillating molecules. Any technique requiring to bind a macromolecule, like a protein, to nano-objects such as nanobeads, nanowires, or surfaces would have an unpredictable effect on the molecular collective oscillations. To go further, we have thus designed other specific methods to detect long-range ED intermolecular forces. A first method conceived is based on the expected change in the diffusion properties of the proteins at different concentrations, in the presence of both suitably activated ED forces and stochastic forces representing the random hits of water molecules on the proteins. The feasibility study of this approach has been carried out via theoretical computations resorting to molecular dynamics simulations. Experimentally, the FCS/FCCS (fluorescence cross correlation spectroscopy) methods that are based on recording the fluctuations of fluorescence signal in a small volume of observation (i.e., a confocal volume in FCS microscopy) have the sensitivity to infer information about the diffusion time through this volume (*41*). The autocorrelation (cross-correlation) function of the detected fluorescence signal is fitted by means of an analytic formula derived by a theoretical model of diffusion. Hence, the diffusion time τ_D, which corresponds to the average time molecules stay within the volume of observation, is obtained and the diffusion coefficient D is simply given by $D = \omega_{xy}^2/4\tau_D$, where ω_{xy}^2 is the lateral waist of the excitation beam focused through the objective of the microscope. This allows us to assess whether the transit time of fluorescent molecules follows a Brownian diffusion law (i.e., resulting from stochastic forces generated by collisions with water molecules) or, instead, a law that possibly combines both ED forces and the stochastic forces just mentioned. A three-step feasibility study has validated this experimental strategy to detect these ED intermolecular forces (*23*, *24*, *25*). In particular, after the results reported in (*24*), the free Brownian diffusion was expected to be markedly reduced by the formation of large molecular clusters when the concentration of the solvated molecules exceeds a critical value. These preliminary results have suggested to experimentally look for this hallmark of the activation of ED interactions. However, a more advanced and thorough investigation of this clustering transition was in order; thus, it has been done in the present work (see section S2.3 of the theoretical part of the Supplementary Materials). By resorting to a semi-analytical model, to molecular dynamics simulations, and to Monte Carlo computations, it is shown that the activation of ED forces entails the existence of a first-order clustering phase transition. This transition between a "dispersed" phase and a "clustered" phase occurs at a critical value of the concentration of actively oscillating out-of-thermal-equilibrium biomolecules, therefore at a critical value of the average intermolecular distance. An independent and complementary experimental possibility of detecting the activation of intermolecular ED forces has been suggested in (*12*). In that case, the frequency of the collective oscillation mode of an isolated macromolecule undergoes a shift when placed close to

another macromolecule oscillating at the same frequency. This shift is inversely proportional to the cube of the intermolecular distance. This remains true for a large number of molecules in solution (see section S3 of the theoretical part of the Supplementary Materials) in which case the frequency shift is found again to be inversely proportional to the cube of the average intermolecular distance. If this represents an experimental cross-check of the diffusion-based approach, then challenge comes a priori from the difficulty in implementing THz spectroscopic measurement of proteins in aqueous solutions due to the strong absorption of water in the THz and sub-THz frequency domains. However, this difficulty is considerably reduced when measurements are performed under out-of-equilibrium conditions. This is distinct from standard spectroscopic measurements, where the incident radiation simultaneously excites the atoms or molecules under study and probes their absorption spectrum by sweeping a range of frequencies. With THz spectroscopy of out-of-equilibrium biomolecules in solution, the analysis is carried out on already active objects (whose vibrations are induced by an internal cascade or interconversion of light), and weak THz radiation is only used to read and detect active vibrations of the biomolecules. Moreover, the absorption of THz radiation by the actively oscillating molecules is much stronger than the absorption of THz radiation by water, thus making molecular absorption features well detectable despite the presence of water.

Two experiments operating under different conditions

In the FCCS setup, the laser beam is focused on a small volume of about 1 fl where a high energy density is attained. This is necessary to excite the collective oscillation of the R-PE molecules during their quick transit through the confocal volume at a transversal diameter of 916 nm. The R-PE molecules efficiently harvest light by means of their 38 fluorochromes within each protein molecule. On the contrary, in the THz spectroscopy setup, a much lower energy density was attained because the laser beam illuminated a large drop of solution of 35 µl. This notwithstanding, the excitation of collective oscillations of both the BSA molecules and of the R-PE molecules, respectively, was attained—without making them cluster—by means of long exposure times. The activation of collective oscillations of the molecules in solution preventing at the same time their clustering (which simply means that the ED forces were unable to overcome the thermal forces) was a necessary condition, and a clustered fraction of the molecules would have completely altered the relationship between frequency shift and concentration. This operating condition was obtained by adjusting the laser power so as to lower the threshold value of the average intermolecular distance of the clustering transition below 500 Å for the R-PE. Moreover, the same laser power density was unable to induce the clustering phase transition of the BSA molecules because the power density was not enough to excite sufficiently strong collective oscillations. This is the reason why the BSA turned out not apt for the experiments based on self-diffusion. The BSA is not naturally sensitive to light, and, to get excited, its collective oscillation mode requires a very long time of light pumping, via the artificially attached fluorochromes, of about 10 min (*19*) to make the corresponding absorption feature sharp enough. Long excitation times are necessary because, in our experimental conditions and for BSA, the rates of energy dissipation and energy input are almost equal. A long time is therefore needed to accumulate enough energy in each protein to make intramolecular nonlinear interaction terms strong enough to activate the

condensation phenomenon. For R-PE, which naturally absorbs light and contains a total of 38 fluorochromes, the process is much faster, and a time of less than 3 s is necessary to observe the formation of clusters in the FCS experiments, whereas in THz experiments, about 1 min (at 50 mW) is needed to begin to detect the spectral features corresponding to collective molecular vibrations and about 4 min are necessary to observe a sharp absorption peak at 71 GHz and about 15 min to excite the second peak at 96 GHz. The physical reason for this is that the phonon condensation phenomenon, which activates the collective vibration of each protein molecule, consists in channelling all the injected energy into the fundamental vibrational mode. Only when the saturation regime is attained does some energy become available also for higher-frequency collective vibrational modes. As above discussed, the phonon condensation is activated after a suitable exposure time of energy injection, that is, when enough energy is accumulated in each molecule. The experimental fact that a much longer exposure time is required to observe the higher frequency peak is thus consistent. In both cases, the mentioned values of time pumping are highly reproducible.

Long illumination times were realized in the THz setup, but this was not possible in the FCS/FCCS setups, where the transit times throughout the confocal volume were exceedingly short to activate the collective oscillations of the BSA molecules despite the high light power density in the confocal volume. In conclusion, let us remark that the ED forces can be active also in the disperse phase when the proteins undergo Brownian diffusion. In other words, even if these forces are not strong enough to make the clustering transition by winning against thermal disorder, they can nevertheless induce the frequency shifts reported in Fig. 4.

Biochemical samples

R-PE was purchased from Merck (52412). BSA conjugated to Alexa Fluor 488 was purchased from Thermo Fisher Scientific (A13100). Samples were prepared by sequential dilutions of proteins in 200 mM NaCl. Their final concentrations were controlled by absorbance measurements (NanoDrop One Spectrophotometer, Thermo Fisher Scientific) at 566 nm for R-PE (ε = 1,960,000 $M^{-1}cm^{-1}$) and at 280 nm for BSA (ε = 43,824 $M^{-1}cm^{-1}$) with a correction factor of 0.11 to account for AF488 at 280 nm.

FCS experiments

Setup

All FCS measurements were performed on a confocal microscope (ALBA FCSTM, from ISS Inc., Champaign, USA) with a picosecond/continuous wave (CW) 488-nm diode laser (BDL-488-SMN, Becker and Hickl, Germany) used at 80 MHz and focused through a water immersion objective (CFI Apo Lambda S 40×/1.25 WI, Nikon). The fluorescence collected by the same objective is split into two paths by a 50/50 beam splitter (Chroma, 21000) and filtered by 525/40-nm bandpass (Semrock, FF02-525/40) before being detected by avalanche photodiodes (SPCM AQRH series, PerkinElmer/Excelitas). Signals are recorded by a multitau hardware correlator (FLEX-02-12D, Correlator.com, Bridgewater, NJ).

Data acquisition

Before each experiment, the laser power is adjusted at the back-aperture objective and the lateral waist value ω was calculated knowing the diffusion coefficient of AF488 [$D_{AF488}(20°C)$ = 409 $\mu m^2/s$ derived in (42)] in aqueous solution at 20°C and according to the equation $\omega^2 = 4D \tau_D$. FFS measurements were performed on samples

in eight-well LAB-TEK chambers (Thermo Scientific Nunc) at given concentrations of proteins diluted in 200 mM NaCl. Five independent experiments were conducted for each condition (protein concentration and laser power) with each individual measure corresponding to a series of 10 measurements lasting 60 s. Different strategies have been previously applied to perform FCS measurements at micromolar concentrations (43, 44). Here, to overcome this concentration limitation, which is mainly due to the detector limits, the collected signal was attenuated by OD filters on the path just after the emission filters. The addition of OD1 or OD1.3 filters with transmission values of 10 and 5%, respectively, allows keeping records with satisfactory amplitude fluctuations and count rates per molecule for reliable analyses. The effectiveness of this experimental approach has been validated with high concentrations of aqueous solutions of the Atto488 dye (figs. S2 and S3). In addition, the use of the FCCS data acquisition modality avoids postpulse artefacts due to spurious photon detection (45).

Data analysis

As mentioned above, all data were collected in FCCS mode for proper experimental analyses. Consequently, we analyze the fluctuations by a CCF defined as

$$G(\tau) = \frac{\langle \delta F_1(t) \delta F_2(t + \tau) \rangle}{\langle F_1 \rangle \langle F_2 \rangle} \tag{5}$$

with $\delta F_1(t)$ and $\delta F_2(t)$ being the signal collected by detectors 1 and 2, respectively. The averages are performed over time. We kept simplest the mathematical model fitting the CCF by using the standard analytic form of the function $G(\tau)$ for a one-component system in a 3D environment which reads as (46)

$$G(\tau) = \frac{1}{N} \left(\frac{1}{(1 + \tau/\tau_D) \sqrt{1 + s^2 \tau/\tau_D}} \right) \tag{6}$$

where N is the average number of molecules, τ_D is the average diffusion time of the tracer through the confocal volume, and s is the structure parameter of the confocal volume, that is, its axial to lateral waist ratio ω_{xy}/ω_z. Still, the fitting accuracy of CCFs with Eq. 6 is no longer very good with high laser power and at high concentrations (fig. S7) because of CCF distortion due to very long transit times of protein clusters. Therefore, the CCFs that are no longer accurately fitted by the standard function $G(\tau)$ are preliminarily smoothed by applying a Savitzky-Golay filter using a polynomial of third degree (red curves on fig. S7). This allows getting reasonable estimates by τ_D as the lag time corresponding to the half-height of the smoothed CCF. Note that when the R-PE concentration exceeds even slightly a clustering critical value, these estimates are fully acceptable and adequate for our purposes. In this case, τ_D suddenly increases by several orders of magnitude with respect to its Brownian value, thus making the details of its estimation irrelevant. The variation of τ_D is also so large that the effects of the high level of noise at short lag times on its estimate do not have any meaningful consequence on the clear evidence of the clustering phase transition.

Confocal video microscopy

The confocal video microscopy images were performed on a confocal microscope (ALBA FCSTM, from ISS Inc., Champaign, USA) with a picosecond/CW 488-nm diode laser (BDL-488-SMN, Becker and Hickl, Germany) used at 80 MHz and focused through a water

immersion objective (CFI Apo Lambda S 40×/1.25 WI, Nikon). The fluorescence collected by the same objective is filtered by a 525/40-nm band pass (Semrock, FF02-525/40) before being detected by avalanche photodiodes (SPCM AQRH series, PerkinElmer/Excelitas). Each 128 × 128 pixel confocal image corresponds to a 30 μm by 30 μm field of view and recorded at a pixel dwell time of 0.1 ms at a rate of 2.8 s per frame. Videos are available as Supplementary Materials (see movies S1 to S4).

THz spectroscopy experiments

Long-range interactions between macromolecules can be highlighted through the dependence of their collective oscillation frequency, lying within the THz domain, on intermolecular distance or concentration. THz near-field spectroscopy allows measuring the occurrence of such collective oscillations if one is able to realize this spectroscopy on proteins immersed in saline solution: a well-known technological roadblock due to the huge absorption of THz radiations by water. We thus have developed two specific setups to overcome this limitation operating in the 0.07- to 0.11-THz domain and in the 0.25- to 0.37-THz range, respectively.

Rectenna-based THz spectroscopy
Setup

For the 0.07- to 0.11-THz band, a CW THz radiation was generated by a Virginia Diodes WR10 source with 25-mW output power. A droplet of 30 to 35 μl of a solution of R-PE (see Materials and Methods) was filed into a 14-pin ceramic dual in-line package forming a cuvette where the rectenna (a bow-tie antenna connected to a GaAs/AlGaAs high-electron-mobility transistor) is placed (Fig. 8A). A plastic (transparent to blue and THz radiations) film was used to seal the system and to reduce evaporation. To excite the proteins, a Spectra Physics blue laser (Excelsior One 488C-50) emitting at 488 nm and delivering a maximum of 50 mW (considering a 1-mm beam diameter, with an optical power density of $\approx 6.4\,\text{W} \cdot \text{cm}^{-2}$) was collimated onto the detector by using a dielectric plane mirror. The laser output power is controlled by a set of optical density filters.

Data acquisition

THz passing through the solution of water, NaCl, and excited protein is detected by the rectenna providing a DC voltage at its loads, proportional to the THz-field intensity. While the dimensions of the rectenna reach half a wavelength (at 0.3 THz), the THz-field is only enhanced in the feed-gap region of the antenna, e.g., within a volume of about 0.2 pl. A hydrophobic, biocompatible, and transparent to both THz and blue radiations varnish was applied to the upper layer of the rectenna. Experiments were done at room temperature.

Data analysis

Normalization procedure, according to the Beer-Lambert law, divides spectra of proteins in solution under illumination I_{R-PEON} by spectra of proteins in solution without illumination $I_{R-PEOFF}$. To obtain spectra of excited proteins only—A is thus proportional to the absorbance coefficient of excited proteins—the result is then divided by the buffer spectra I_{NaCl} (also with and without illumination)

$$A = \log\left(\frac{I_{R-PE_{ON}} \div I_{R-PE_{OFF}}}{I_{NaCl_{ON}} \div I_{NaCl_{OFF}}}\right) \qquad (7)$$

The Savitsky-Golay smoothing was used at the end to smooth curves, with 15 points of window and a polynomial order of 2 [see an example of data treatment in fig. S9].

Technical limitations

The absence of the second peak in Fig. 2 (and in the related fig. S9) is due to the difficulty of working at high input power and long acquisition time, as used for Fig. 3. This would make the stabilization of temperature and the control of evaporation (thus of protein concentration) hard over such a small solution volume and during an overall acquisition time of about 90 min that would be needed to observe also the second peak in Fig. 2 (instead of 8 to 9 min to work it out in its present form, with each spectrum having been recorded in 1.6 min as is the case of fig. S9).

Microwire-based probe
Setup

For the 0.25- to 0.37-THz band, CW-THz radiation is produced by a signal generator extension (SGX) module designed by Virginia Diodes Inc. Module WR9.0 (82 to 125 GHz) SGX was used with external multiplier WR2.8 to extend the frequency coverage to 0.25 to 0.37 THz with an average power of 1 mW. The radiation emitted is then collimated and focused by polytetrafluoroethylene lenses on the biological sample. Optical excitation, represented by a blue laser and an ultraviolet (UV) lamp, was used to excite different components of the protein under study. Thus, for the optical excitation of fluorochromes, a Cobolt 06-MLD laser was used, emitting an output power of 40 mW at the wavelength of 488 nm. Optical excitation of aromatic amino acids included in the protein was performed using LED M275L4 produced by ThorLabs at a wavelength of 275 nm and a typical output power of 60 mW. Because of its large numerical aperture (0.86), UV-coated lenses were used to collimate and focus the radiation onto the sample. Thus, a spot size of about 1 cm in diameter was achieved. A micro-coaxial near-field wire (fig. S8B) is inserted inside a metallic rectangular waveguide to allow a modal transition from TM01 Sommerfeld's mode to TE01 waveguide mode. The probe is capable of highly localized detection of the longitudinal component of the electric field (47) due to the subwave diameter of the wire around 10 μm at the tip into the volume of about 4 pl.

Data acquisition

A specific sample holder was also designed. It is constituted by a plastic cylinder, transparent to UV, blue, and THz radiations and resistant to UV radiation with a diameter of 7 mm and a volume of 53 μl. At its bottom, a 130-μm-thick glass was used, through which laser excitation was performed. To avoid evaporation and, as a consequence, changes in protein concentration during the experiment, the sample was covered by a plastic film with a thickness of 5 μm, allowing the wire to pass through it without damage.

Data analysis

Regarding the normalization, the same procedure as in rectenna experiments has been followed, according to the Beer-Lambert law, to obtain spectra of excited proteins only. However, since in this frequency band (0.25 to 0.37 THz) the signal-to-noise ratio is poor due to high absorption by water molecules, a specific data processing and normalization procedure (using a band-stop Fourier transform filtering and Lorentz functions fitting) has been followed to extract a usable signal and frequencies of collective-oscillation resonances.

It is thus possible to observe the evolution of the absorption-peak amplitude as a function of the duration of illumination. Where considered as absorption peaks, those whose height and area are increasing continuously with time. Time (up to 1 hour) and concentration (from 750 to 60,000 nM) dependences of the THz spectra have been characterized.

SUPPLEMENTARY MATERIALS

Supplementary material for this article is available at https://science.org/doi/10.1126/sciadv.abl5855

View/request a protocol for this paper from *Bio-protocol*.

REFERENCES AND NOTES

1. K. Venkatesan, J.-F. Rual, A. Vazquez, U. Stelzl, I. Lemmens, T. Hirozane-Kishikawa, T. Hao, M. Zenkner, X. Xin, K.-I. Goh, M. A. Yildirim, N. Simonis, K. Heinzmann, F. Gebreab, J. M. Sahalie, S. Cevik, C. Simon, A.-S. de Smet, E. Dann, A. Smolyar, A. Vinayagam, H. Yu, D. Szeto, H. Borick, A. Dricot, N. Klitgord, R. R. Murray, C. Lin, M. Lalowski, J. Timm, K. Rau, C. Boone, P. Braun, M. E. Cusick, F. P. Roth, D. E. Hill, J. Tavernier, E. E. Wanker, A.-L. Barabási, M. Vidal, An empirical framework for binary interactome mapping. *Nat. Methods* **6**, 83–90 (2009).
2. L. Bonetta, Interactome under construction. *Nature* **468**, 851–852 (2010).
3. M. Gori, I. Donato, E. Floriani, I. Nardecchia, M. Pettini, Random walk of passive tracers among randomly moving obstacles. *Theor. Biol. Med. Model.* **13**, 13–33 (2016).
4. D. S. Banks, C. Fradin, Anomalous diffusion of proteins due to molecular crowding. *Biophys. J.* **89**, 2960–2971 (2005).
5. Y. Golan, E. Sherman, Resolving mixed mechanisms of protein subdiffusion at the T cell plasma membrane. *Nat. Commun.* **8**, 15851–15866 (2017).
6. S. F. Banani, H. O. Lee, A. A. Hyman, M. K. Rosen, Biomolecular condensates: Organizers of cellular biochemistry. *Nat. Rev. Mol. Cell Biol.* **18**, 285–298 (2017).
7. J. Berry, C. P. Brangwynne, M. Haataja, Physical principles of intracellular organization via active and passive phase transitions. *Rep. Prog. Phys.* **81**, 046601–046643 (2018).
8. L. J. Sweetlove, A. R. Fernie, The role of dynamic enzyme assemblies and substrate channelling in metabolic regulation. *Nat. Commun.* **9**, 2136–2148 (2018).
9. O. I. Kulaeva, E. V. Nizovtseva, Y. S. Polikanov, S. V. Ulianov, V. M. Studitsky, Distant activation of transcription: Mechanisms of enhancer action. *Mol. Cell. Biol.* **32**, 4892–4897 (2012).
10. J. Wang, X. Meng, H. Chen, C. Yuan, X. Li, Y. Zhou, M. Chen, Exploring the mechanisms of genome-wide long-range interactions: Interpreting chromosome organization. *Brief. Funct. Genomics* **15**, 385–395 (2016).
11. I. Wheeldon, S. D. Minteer, S. Banta, S. C. Barton, P. Atanassov, M. Sigman, Substrate channelling as an approach to cascade reactions. *Nat. Chem.* **8**, 299–309 (2016).
12. J. Preto, M. Pettini, J. A. Tuszynski, Possible role of electrodynamic interactions in long-distance biomolecular recognition. *Phys. Rev. E* **91**, 052710–052728 (2015).
13. J. R. de Xammar Oro, G. Ruderman, J. R. Grigera, Electrodynamics of interactions in electrolyte media. Possible consequences in biological functions. *Biophysics* **53**, 195–198 (2008).
14. J. C. Maxwell, *A Treatise on Electricity & Magnetism* (Dover Publications Inc., New-York, 1954).
15. P. Debye, Reaction rates in ionic solutions. *Trans. Electrochem. Soc.* **82**, 265–272 (1942).
16. R. M. Noyes, Effects of diffusion rates on chemical kinetics. *Prog. React. Kinet.* **1**, 129 (1961).
17. H. Fröhlich, Long-range coherence in biological systems. *Rivista Nuovo Cimento* **7**, 399–418 (1977).
18. A. Salam, *Molecular Quantum Electrodynamics* (John Wiley and Sons, Inc., New Jersey, 2010).
19. I. Nardecchia, J. Torres, M. Lechelon, V. Giliberti, M. Ortolani, P. Nouvel, M. Gori, Y. Meriguet, I. Donato, J. Preto, L. Varani, J. Sturgis, M. Pettini, Out-of-equilibrium collective oscillation as phonon condensation in a model protein. *Phys. Rev. X* **8**, 031061–031084 (2018).
20. P. Kurian, G. Dunston, J. Lindesayk, How quantum entanglement in DNA synchronizes double-strand breakage by type II restriction endonucleases. *J. Theor. Biol.* **391**, 102–112 (2016).
21. P. Kurian, A. Capolupo, T. J. A. Craddock, G. Vitiello, Water-mediated correlations in DNA-enzyme interactions. *Phys. Lett. A* **382**, 33–43 (2018).
22. Z. Zhang, G. S. Agarwal, M. O. Scully, Quantum fluctuations in the Fröhlich condensate of molecular vibrations driven far from equilibrium. *Phys. Rev. Lett.* **122**, 158101–158107 (2019).
23. J. Preto, E. Floriani, I. Nardecchia, P. Ferrier, M. Pettini, Experimental assessment of the contribution of electrodynamic interactions to long-distance recruitment of biomolecular partners: Theoretical basis. *Phys. Rev. E* **85**, 041904–041916 (2012).
24. I. Nardecchia, L. Spinelli, J. Preto, M. Gori, E. Floriani, S. Jaeger, P. Ferrier, M. Pettini, Experimental detection of long-distance interactions between biomolecules through their diffusion behavior: Numerical study. *Phys. Rev. E* **90**, 022703–022717 (2014).
25. I. Nardecchia, M. Lechelon, M. Gori, I. Donato, J. Preto, E. Floriani, S. Jaeger, S. Mailfert, D. Marguet, P. Ferrier, M. Pettini, Detection of long-range electrostatic interactions between charged molecules by means of fluorescence correlation spectroscopy. *Phys. Rev. E* **96**, 022403–022416 (2017).
26. S. Olmi, M. Gori, I. Donato, M. Pettini, Collective behavior of oscillating electric dipoles. *Sci. Rep.* **8**, 15748–15760 (2018).
27. W. R. Chang, T. Jiang, Z. L. Wan, J. P. Zhang, Z. X. Yang, D. C. Liang, Crystal structure of R-phycoerythrin from *Polysiphonia urceolata* at 2.8 Å resolution. *J. Mol. Biol.* **262**, 721–731 (1996).
28. R. D. Blevins, *Formulas for Natural Frequency and Mode Shape* (Van Nostrand Reinhold Company, New-York, 1979).
29. S. Perticaroli, J. D. Nickels, G. Ehlers, H. O'Neill, Q. Zhang, A. P. Sokolov, Secondary structure and rigidity in model proteins. *Soft Matter* **9**, 9548–9556 (2013).
30. F. Schuster, D. Coquillat, H. Videlier, M. Sakowicz, F. Teppe, L. Dussopt, B. Giffard, T. Skotnicki, W. Knap, Broadband terahertz imaging with highly sensitive silicon CMOS detectors. *Opt. Express* **19**, 7827–7832 (2011).
31. R. Van Wijk, E. P. A. Van Wijk, J. Pang, M. Yang, Y. Yan, J. Han, Integrating ultra-weak photon emission analysis in mitochondrial research. *Front. Physiol.* **11**, 717 (2020).
32. G. L. Celardo, M. Angeli, T. J. A. Craddock, P. Kurian, On the existence of superradiant excitonic states in microtubules. *New J. Phys.* **21**, 023005 (2019).
33. M. Stöhr, A. Tkatchenko, Quantum mechanics of proteins in explicit water: The role of plasmon-like solute-solvent interactions. *Sci. Adv.* **5**, eaax0024 (2019).
34. D. Tischer, O. D. Weiner, Illuminating cell signalling with optogenetic tools. *Nat. Rev. Mol. Cell Biol.* **15**, 551–558 (2014).
35. N. Veljkovic, S. Glisic, V. Perovic, V. Veljkovic, The role of long-range intermolecular interactions in discovery of new drugs. *Expert Opin. Drug Discov.* **6**, 1263–1270 (2011).
36. P. C. Painter, L. E. Mosher, C. Rhoads, Low-frequency modes in the Raman spectra of proteins. *Biopolymers* **21**, 1469–1472 (1982).
37. P. C. Painter, L. Mosher, C. Rhoads, Low-frequency modes in the Raman spectrum of DNA. *Biopolymers* **20**, 243–247 (1981).
38. H. Fröhlich, Long-range coherence and energy storage in biological systems. *Int. J. Quantum Chem.* **2**, 641–649 (1968).
39. H. Fröhlich, Long range coherence and the action of enzymes. *Nature* **228**, 1093 (1970).
40. H. Fröhlich, Selective long range dispersion forces between large systems. *Phys. Lett. A* **39**, 153–154 (1972).
41. E. Haustein, P. Schwille, Fluorescence correlation spectroscopy: Novel variations of an established technique. *Annu. Rev. Biophys. Biomol. Struct.* **36**, 151–169 (2007).
42. Z. Petrášek, P. Schwille, Precise measurement of diffusion coefficients using scanning fluorescence correlation spectroscopy. *Biophys. J.* **94**, 1437–1448 (2008).
43. T. Laurence, S. Ly, F. Bourguet, N. O. Fischer, M. A. Coleman, Fluorescence correlation spectroscopy at micro-molar concentrations without optical nanoconfinement. *J. Phys. Chem.* **118**, 9662–9667 (2014).
44. S. Khatua, H. Yuan, M. Orrit, Enhanced-fluorescence correlation spectroscopy at micro-molar dye concentration around a single gold nanorod. *Phys. Chem. Chem. Phys.* **17**, 21127–21132 (2015).
45. M. Zhao, L. Jin, B. Chen, Y. Ding, H. Ma, D. Chen, After pulsing and its correction in fluorescence correlation spectroscopy experiments. *Appl. Optics* **42**, 4031–4036 (2003).
46. D. Magde, E. Elson, A. Hyman, W. Webb, Fluorescence correlation spectroscopy. II. An experimental realization. *Biopolymers* **13**, 29–61 (1974).
47. F. Keilmann, FIR microscopy. *Infrared Phys. Techno.* **36**, 217–224 (1995).
48. F. M. Richards, Areas, volumes, packing, and protein structure. *Annu. Rev. Biophys. Bioeng.* **6**, 151–176 (1977).
49. H. Durchschlag, Determination of the partial specific volume of conjugated proteins. *Colloid Polym. Sci.* **267**, 1139–1150 (1989).
50. P.-H. Chavanis, Phase transitions in self-gravitating systems: Self-gravitating fermions and hard-sphere models. *Phys. Rev. E* **65**, 056123 (2002).
51. E. R. Likhachev, Dependence of water viscosity on temperature and pressure. *Tech. Phys.* **48**, 514–515 (2003).
52. J. N. Israelachvili, *Intermolecular and Surface Forces* (Academic press, 2011).
53. M. Farnum, C. Zukoski, Effect of glycerol on the interactions and solubility of bovine pancreatic trypsin inhibitor. *Biophys. J.* **76**, 2716–2726 (1999).
54. M. Lund, B. Jönsson, A mesoscopic model for protein-protein interactions in solution. *Biophys. J.* **85**, 2940–2947 (2003).
55. E. Faraji, R. Franzosi, S. Mancini, M. Pettini, Energy transfer to the phonons of a macromolecule through light pumping. *Sci. Rep.* **11**, 6591–6605 (2021).
56. I. Y. Torshin, R. W. Harrison, Charge centers and formation of the protein folding core. *Proteins* **43**, 353–364 (2001).
57. S. Tsonchev, G. C. Schatz, M. A. Ratner, Screened multipole electrostatic interactions at the Debye–Hückel level. *Chem. Phys. Lett.* **400**, 221–225 (2004).
58. B. Alberts, A. Johnson, J. Lewis, P. Walter, M. Raff, K. Roberts, *Molecular Biology of the Cell 4th Edition: International Student Edition* (Routledge, 2002).
59. J. P. T. Zaragoza, A. Nguy, N. Minnetian, Z. Deng, A. T. Iavarone, A. R. Offenbacher, J. P. Klinman, Detecting and characterizing the kinetic activation of thermal networks in proteins: Thermal transfer from a distal, solvent-exposed loop to the active site in soybean lipoxygenase. *J. Phys. Chem. B* **123**, 8662–8674 (2019).
60. A. Campa, T. Dauxois, S. Ruffo, Statistical mechanics and dynamics of solvable models with long-range interactions. *Phys. Rep.* **480**, 57–159 (2009).
61. V. V. Shcherbakov, Y. M. Artemkina, E. N. Korotkova, Dielectric properties and high-frequency conductivity of the sodium chloride-water system. *Russ. J. Inorg. Chem.* **59**, 922–926 (2014).

Science Advances

Experimental evidence for long-distance electrodynamic intermolecular forces

Mathias LechelonYoann MeriguetMatteo GoriSandra RuffenachIlaria NardecchiaElena FlorianiDominique CoquillatFrédéric TeppeSébastien MailfertDidier MarguetPierre FerrierLuca VaraniJames SturgisJeremie TorresMarco Pettini

View the article online
https://www.science.org/doi/10.1126/sciadv.abl5855
Permissions
https://www.science.org/help/reprints-and-permissions

Use of think article is subject to the Terms of service